Blistering Pattern and Formation of Nanofibers in Capillary Thinning of Polymer Solutions

R. Sattler,[1,*] C. Wagner,[1] and J. Eggers[2]

[1]*Experimentalphysik, Universität des Saarlandes, Postfach 151150, 66041 Saarbrücken, Germany*
[2]*School of Mathematics, University of Bristol, University Walk, Bristol BS8 1TW, United Kingdom*

When a dilute polymer solution experiences capillary thinning, it forms an almost uniformly cylindrical thread, which we study experimentally. In the last stages of thinning, when polymers have become fully stretched, the filament becomes prone to instabilities, of which we describe two: a novel breathing instability, originating from the edge of the filament, and a sinusoidal instability in the interior, which ultimately gives rise to a blistering pattern of beads on the filament. We describe the linear instability with a spatial resolution of 80 nm in the disturbance amplitude. For sufficiently high polymer concentrations, the filament eventually separates out into a ''solid'' phase of entangled polymers, connected by fluid beads. A solid polymer fiber of about 100 nm thickness remains, which is essentially permanent.

When a drop falls from a faucet, surface tension drives the fluid motion toward breakup in finite time, and a drop separates. This pinch-off occurs in a localized fashion [1], and the neighborhood of the point of breakup is described by a similarity solution [2]. If however very small amounts of high molecular weight polymer are added, an almost perfectly cylindrical thread is formed instead [3–6]. The reason is that wherever there is a local decrease in radius, fluid elements are stretched, and the polymers along with it. This will increase the extensional viscosity of the fluid-polymer mixture [7], and further flow is inhibited, thus forming a uniform and stable filament.

For most of this Letter, we produce a filament by placing a drop of liquid between two solid plates, which are rapidly drawn apart [8]. (In a simple and educational version of this experiment, a drop of saliva is placed between thumb and index finger.) A single filament forms between the plates, which thins as surface tension drains fluid from the filament, and into two roughly hemispherical reservoirs at the end plates.

This Letter addresses the later stages of the thinning of the polymeric filament, when polymers have come close to their full extension. Thus the mechanism that formerly used to stabilize the thread is no longer effective, and tiny beads begin to appear on the filament (see Fig. 1, images 5 and 6) [9]. We will refer to this process central to the present study as ''blistering.'' This instability occurs when the filament is only in the order of several microns in radius, requiring extreme spatial resolution. If the concentration of polymer is sufficiently high, the filament can become very long lived compared to the time scale of a dissolved polymer.

Theoretically, the period of exponential thinning has recently been described within a long-wavelength description [6]. Nonetheless, the full three-dimensional, axisymmetric problem remains unsolved. The effect of finite polymer extensibility has been studied numerically in [10], once more using a long-wavelength model. The

filament is found to fail near its end via a localized similarity solution, in contrast to the much more complex scenario found here. The first clear experimental description of blistering is found in [11,12], which focuses on the later stages of the instability, in the course of which droplets with a hierarchy of sizes are found. We first focus on the *onset* of the blistering instability, for which widely diverging theoretical explanations have been expressed in the past [6,10,11,13].

The observations we report here have general validity for a variety of polymer-solvent systems. Experiments have been performed with polyethylenoxide (PEO) in water, PEO in xylol, human saliva, polyacryl-co-
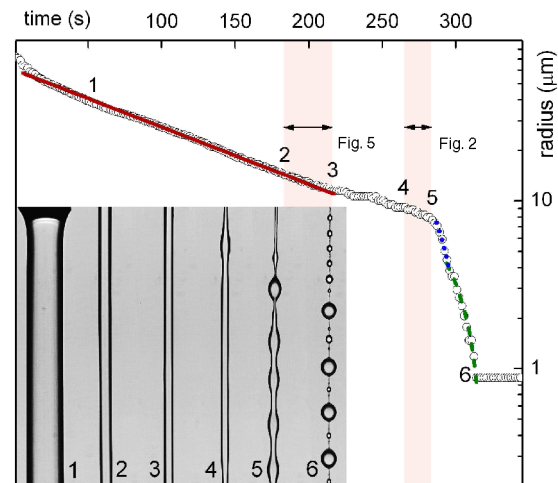

FIG. 1 (color online).   The minimum radius h_{min} as a function of time. Not all data points are shown. Between numbers 1 and 3, the curve is well described by $h_{min}(t) = h_0 \exp(-t/\tau)$ with $\tau = 130 \pm 30$ ms (red, straight line). A plateau is reached between 3 and 4 which is associated with an instability near the end plates, followed by rapid pinching. Between 5 and 6 the curve can be approximated with two linear laws (dotted blue and dashed green lines). For further explanation see text.

acrylicacid in water-sugar, polysterol in diethyl phthalate and dimethyl furane. This covers a wide range of different polymers of different polarities and with vapor pressures ranging between less than 1 Pa and more than 2000 Pa. However, we focus here on PEO as an established model system, and details on other systems will be published elsewhere. The experiments were performed with aqueous solutions of PEO of molecular weights $M_W = (1–8) \times 10^6$ amu and concentrations $0.010 \leq c \leq 0.2$ wt %. While the formation of a filament and its subsequent instability could be observed well below the overlap concentration [7] of polymers, we focused on higher concentrations, as the process is slower and easier to observe. Our reference system has $M_W = 4 \times 10^6$ amu and $c = 0.2$ wt %, with $c_{ov} = 0.07$ wt % the overlap concentration. The samples were characterized with a Thermo Haake MARS rheometer using cone plate geometries. The zero shear viscosity was $\eta_0 \approx 50$ mPa s and in the range of shear rates $0.1 \leq \dot{\gamma} \leq 2000$ shear thinning was present down to a value of $\eta_\infty \approx 4$ mPa s [14]. The surface tension was determined by the pendant drop method to $\gamma \sim 60.9$ mN/m.

We used a capillary breakup device similar to the one described in [11,15]. This setup is also commercially available to measure the extensional rheology of suspensions (CaBER, Thermo Fisher Scientific, Karlsruhe, Germany). To ensure maximum reproducibility, we used the following protocol: plates of diameter $d = 2$ mm were held at a distance of $l = 2.5$ mm for the purpose of relaxation for several seconds. Then the plates are drawn to $l = 3.5$ mm within 40 ms, only slightly exceeding the limit at which a capillary bridge of the solvent experiences a Rayleigh-Plateau instability and breakup. The thinning process is observed with an IDT X-Vision X3 digital high-speed video camera with Nikon Microscope objectives of up to 20× magnification. At the highest magnification, the diffraction limited resolution is 0.6 μm, and depth of field is 5 μm. A Halogen backlight allows frame rates up to 6000 frames per second and exposure times down to 10 μs.

Figure 1 shows a typical recording of the thread radius $h_{min}(t)$ in the cylindric region in a semilogarithmic plot. For plug flow in a cylindrical filament, the elongation rate is determined from $\dot{\epsilon} = -2d \ln h/dt$; thus, $\dot{\epsilon}$ is constant for most of the filament thinning, which follows an exponential law (the regime between 1 and 2 in Fig. 1) [4]. The axial stress σ_{zz} supported by the polymers balances the increasing capillary pressure γ/h_{min}, which means that the extensional viscosity $\eta_E \equiv \sigma_{zz}/\dot{\epsilon} = \gamma/(h_{min}\dot{\epsilon})$ also increases exponentially. At 3 (see Fig. 1) the thread radius first has a plateau, and then thinning accelerates again. The reason for the acceleration is that the polymers have almost reached their maximum extension, so their extensional viscosity can no longer increase. But this means that $\dot{\epsilon}$ has to increase rapidly, implying a steep increase in the
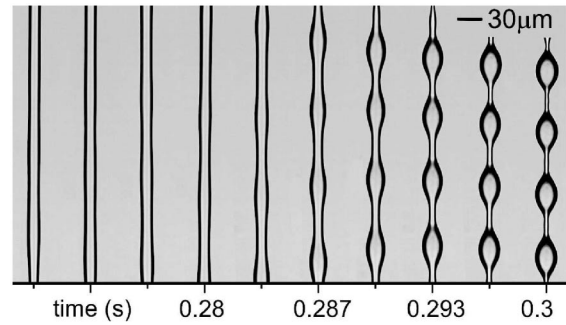

FIG. 2. Growth of a sinusoidal instability of the viscoelastic filament that develops into a group of droplets on the thinning filament. The spacing of the pictures is 300^{-1} s. The time window between 4 and 5 in Fig. 1 is represented by the images up to 0.287 s showing the range of exponential growth.

slope of $\log h(t)$, as seen in Fig. 1. Once η_E has reached a plateau, which we estimate at $h_{min} \approx 12$ μm to be $\eta_E (12 \ \mu m) \approx 330$ Pa s, the filament behaves essentially like a Newtonian fluid [10], and is thus subject to a capillary instability [16], as confirmed below. Note that this value of the extensional viscosity corresponds to an increase by 5 orders of magnitude over $\eta_{water} = 10^{-3}$ Pa s of the solvent.

Before we describe the novel instability that occurs between 2 and 3 in Fig. 1, which is localized near the end plates, we concentrate on the subsequent spatially uniform, *linear* instability which is shown in Fig. 2 (between 4 and 5 in Fig. 1). At first, no oscillations are visible on the images of Fig. 2; however, as seen in Fig. 3, we are
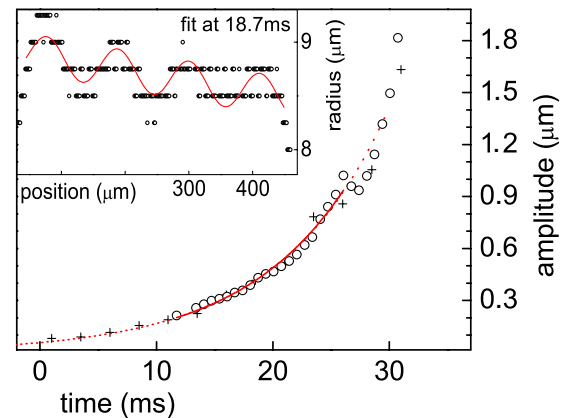

FIG. 3 (color online). Main: The growth of the amplitude of a sinusoidal surface deformation on a filament of radius $R_0 = 10$ μm. The origin of the time axis has been shifted relatively to Fig. 1. Circles and crosses are experimental data of two different runs; from the latter we were able to detect amplitudes as low as 80 nm. The straight line and the dotted line are exponential fits, giving an inverse growth rate of $\omega = 9.3 \pm 0.1$ ms. Inset: The sinusoidal surface deformation at $t = 18.7$ ms. Points are experimental data and the solid line is a fit with a sine and a linear offset. The selected wavelength is $\lambda/R_0 = 12 \pm 0.9$.

able to resolve perturbations down to an amplitude of $A = 80$ nm, corresponding to significant superresolution [17]. This is done by fitting the profile with a sine function with wave number, phase, and amplitude as free parameters over many wavelengths (see inset). The algorithm converged down to the stated maximum resolution. The last four pictures of Fig. 2 show the beginning of the nonlinear stages of the instability, finally leading to the formation of smaller secondary droplets [11,12]. In the main panel of Fig. 3 we plot the growth of the sinusoidal approximation over time, an example of which is shown in the inset. Over more than a decade, the growth is very well described by an exponential, providing a clear signature of a *linear instability*, which develops uniformly in space.

From a fit to the exponential, we find an inverse growth rate of $1/\omega = 9.3 \pm 0.1$ ms. Linear stability of a viscous fluid thread [16] predicts $\omega = \gamma/(6R_0\eta_{\text{eff}})$, which gives an estimated extensional viscosity of $\eta_{\text{eff}} = 9$ Pa s ± 2, more than 1 order of magnitude smaller than the extensional viscosity η_E (12 μm) estimated above. At the same time, we are able to fit—as expected [16]—a *linear* law $h_{\text{min}} = -0.44 \times 10^{-3}$ m/sΔt in the range $8 > h_{\text{min}} > 4$ μm. Comparing to the law $h_{\text{min}} = 0.07\gamma/\eta_{\text{eff}}\Delta t$ for viscous pinching [18], this gives $\eta_{\text{eff}} = 10$ Pa s, which agrees nicely. We do not have a ready explanation for the discrepancy between η_{eff} and η_E (12 μm). Among possible explanations are nonuniformities in the polymer concentration (see below), and transient relaxation of polymer stresses during the plateau between 3 and 4 in Fig. 1, when there is no flow. A kink in the linear shrinking behavior at $h_{\text{min}} \sim 3.8$ μm toward a less steep slope of -0.17×10^{-3} m/s could either be seen as a first indication for the onset of a draining process discussed below or as a transition from the viscous to the inertial-viscous pinch-off regime [18].

The formation of successive generations of beads has already been studied extensively [11,12]; we focus on the very final stages of the thinning process, when the formation of new beads has come to rest (6 in Fig. 1). If the polymer concentration was greater than 1000 ppm, the filament connecting two beads *never* breaks, and a pattern as shown in Fig. 4(a) is formed. What is remarkable is that most beads are off center with respect to the filament. Comparison with the problem of fluid drops on a fiber [19] shows that there must be a *finite* contact angle between the drops and the filament for such a symmetry breaking to occur. In other words, the thin filament must have formed a (solid) phase different from that of the drops [20].

To confirm this idea, we produced the scanning-electron-microscopy (SEM) images shown in Fig. 4. Object slides were pulled quickly through the liquid bridge, before the accumulated elastic stress would lead it to retract into a single droplet. Figure 4(b) shows two remnants of two droplets being connected by a persistent thin thread. Increased magnification [4(c) and 4(d)] allowed us to
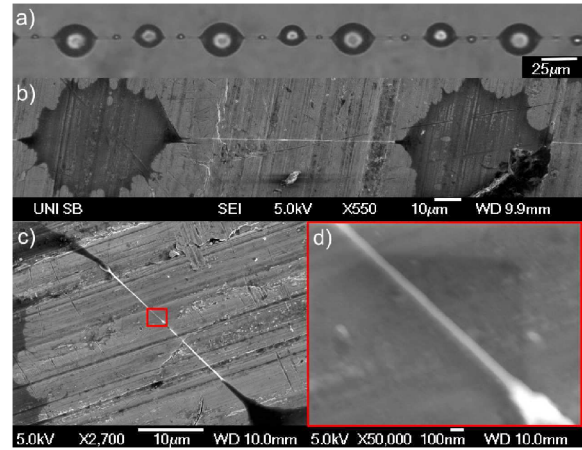

FIG. 4 (color online).   (a) The final state of the filament. Beads are formed off center relative to the thread. (b) SEM image of two beads, connected by a thread (intermediate resolution). The structure was caught and dried upon the substrate (c) Another example of the structure, the red box indicating a close-up at high magnification shown in (d). The diameter of the fiber can be as small as 70 nm.

estimate the diameter of the fiber as 75–150 nm. Assuming a constant polymer concentration of the solution, and taking for the fiber the density of PEO, the amount of polymer in such a fiber equals to a 2000 ppm solution with a diameter of 3 μm, thereby representing a lower bound for the onset of the concentration process that leads to this solid fiber, but which is likely to start earlier. Our physical picture is that polymers become entangled, while solvent drains from the filament, leading to even higher polymer concentration and increased entanglement; i.e., a flow induced phase separation takes place [21]. Further evidence for this concentration process was already found in [22], where birefringence measurements were performed to examine molecular conformations in the breakup process. We can *exclude* evaporation to be a factor in the formation of solid fibers, based on our estimates of evaporation rates, as well as preliminary experiments in a two-fluid system.

Finally, we would like to describe the transition regime (between 2 and 3 in Fig. 1) where an instability of the homogenous elongational flow originates from the boundary, and is reminiscent of phenomena reported in [13]. The transition region at the edge of the filament was described in detail in [6] for the case that polymers are far from stretched. At full stretch, the transition region constricts [as seen in the last shape in the inset of Fig. 5 (full triangles)], thus inhibiting the flow out of the filament. The most sensitive probe for the flow is tiny bubbles inside the filament, whose trajectories are shown in Fig. 5. During the constriction phase, the flow stops, and the tracer positions form a plateau. In the absence of flow, polymers relax inside the filament, and elastic stresses are eventually no longer able to sustain the capillary pressure. Fluid from the
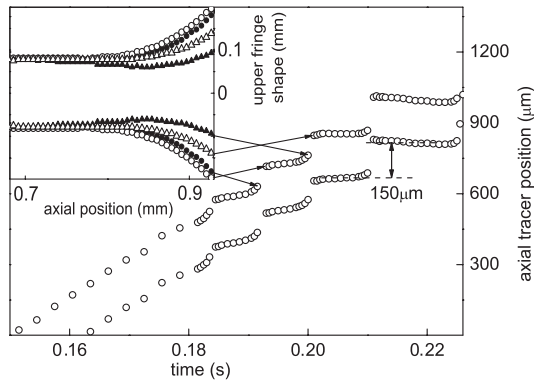
FIG. 5. Trajectories of two bubbles in the filament; they move in parallel, indicating uniform flow inside the filament. First the bubbles are convected by the extensional flow produced by the thinning. Then their position undergoes a sequence of plateaus, associated with consecutive contractions and relaxations—the "breathing" at the very end of the filament, shown in the inset. The breathing correspondents to the red shaded region between 2 and 3 in Fig. 1. At 3, the bubbles run out of the field of view.

filament empties into the end cap, causing a sudden flow, which appears as a jump in bubble position in Fig. 5. The process repeats itself periodically, on a time scale that increases from step to step, but which is of the same order of magnitude as the polymer relaxation time.

The height of the final jump gives a characteristic length scale of 150 μm, which is comparable to the wavelengths of periodic disturbances on the filament (Fig. 2). In principle, each of the plateaus shown in Fig. 5 should result in a corresponding plateau in $h_{\min}$. However, the plateaus are too small to be resolved, apart from the last two between 3 and 4 in Fig. 1. At the end of the plateaus the filament shrinks again by draining liquid into the reservoir at the end plates or into a large bead that typically forms in the middle of the filament; see [9].

In conclusion, we have demonstrated three key phenomena: (i) Between 2 and 3 in Fig. 1, the trumpet-shaped transition region connecting the filament to the reservoirs constricts periodically, interrupting the flow. (ii) The blistering instability of the filament, which leads to beads, is a linear capillary instability (between 4 and 5 in Fig. 1). As the polymers reach full stretch, their contribution is once more Newtonian, but with a viscosity that is many times that of the unstretched state. (iii) Using electron microscopy, we provide evidence that the filament remains intact in its latest stages, because polymer strands become sufficiently concentrated to become solidlike. The most compelling evidence for this fact is that the contact angle

between the thread and the beads sitting on it becomes *finite*. Existing theoretical models are clearly inadequate in addressing this polymer behavior at full stretch.

*r.sattler@mx.uni-saarland.de
[1] A. Cordoba, D. Cordoba, C. L. Fefferman, and M. A. Fontelos, Adv. Math. **187**, 228 (2004).
[2] J. Eggers, Phys. Rev. Lett. **71**, 3458 (1993).
[3] A. V. Bazilevskii, V. M. Entov, and A. N. Rozhkov, Sov. Phys. Dokl. **26**, 333 (1981).
[4] Y. Amarouchene, D. Bonn, J. Meunier, and H. Kellay, Phys. Rev. Lett. **86**, 3558 (2001).
[5] C. Wagner, Y. Amarouchene, D. Bonn, and J. Eggers, Phys. Rev. Lett. **95**, 164504 (2005).
[6] C. Clasen, J. Eggers, M. A. Fontelos, J. Li, and G. H. McKinley, J. Fluid Mech. **556**, 283 (2006).
[7] R. B. Bird, R. C. Armstrong, and O. Hassager, *Dynamics of Polymeric Liquids* (Wiley, New York, 1987), Vols. 1, 2.
[8] S. L. Anna and G. H. McKinley, J. Rheol. (N.Y.) **45**, 115 (2001).
[9] See EPAPS Document No. E-PRLTAO-100-064817 for a movie of the blistering process. For more information on EPAPS, see http://www.aip.org/pubservs/epaps.html.
[10] J. Li and M. A. Fontelos, Phys. Fluids **15**, 922 (2003).
[11] M. S. N. Oliveira and G. H. McKinley, Phys. Fluids **17**, 071704 (2005).
[12] M. S. N. Oliveira, R. Yeh, and G. H. McKinley, J. Non-Newtonian Fluid Mech. **137**, 137 (2006).
[13] H. C. Chang and E. A. Demekhin, J. Fluid Mech. **380**, 233 (1999).
[14] The solution is similar to the one described in Ref. [12] where a more extensive rheological description can be found.
[15] L. E. Rodd, T. P. Scott, J. J. Cooper-White, and G. H. McKinley, Applied Rheology **15**, 12 (2005).
[16] J. Eggers, Rev. Mod. Phys. **69**, 865 (1997).
[17] B. R. Hunt, Int. J. Imaging Syst. Technol. **6**, 297 (1995).
[18] A. Rothert, R. Richter, and I. Rehberg, New J. Phys. **5**, 59 (2003).
[19] B. J. Carroll, Langmuir **2**, 248 (1986).
[20] D. F. James and J. H. Saringer, J. Fluid Mech. **97**, 655 (1980).
[21] T. Kume, T. Hashimoto, T. Takahashi, and G. G. Fuller, Macromolecules **30**, 7232 (1997), and references therein.
[22] R. Sattler, A. Kityk, and C. Wagner, Phys. Rev. E **75**, 051805 (2007).